The Astrophysical Journal, 832:70 (10pp), 2016 November 20 doi:10.3847/0004-637X/832/1/70

THE *CHANDRA* COSMOS LEGACY SURVEY: CLUSTERING OF X-RAY-SELECTED AGNs AT $2.9 \leqslant z \leqslant 5.5$ USING PHOTOMETRIC REDSHIFT PROBABILITY DISTRIBUTION FUNCTIONS

V. Allevato[1,2], F. Civano[3,4], A. Finoguenov[1,2], S. Marchesi[3,4,5], F. Shankar[6], G. Zamorani[7], G. Hasinger[8], M. Salvato[9], T. Miyaji[10], R. Gilli[5], N. Cappelluti[3], M. Brusa[5,7], H. Suh[8], G. Lanzuisi[5,7], B. Trakhtenbrot[11], R. Griffiths[12], C. Vignali[5,7], K. Schawinski[11], and A. Karim[13]

[1] Department of Physics, University of Helsinki, Gustaf Hällströmin katu 2a, FI-00014 Helsinki, Finland
[2] University of Maryland, Baltimore County, 1000 Hilltop Circle, Baltimore, MD 21250, USA
[3] Yale Center for Astronomy and Astrophysics, 260 Whitney Avenue, New Haven, CT 06520, USA
[4] Harvard Smithsonian Center for Astrophysics, 60 Garden Street, Cambridge, MA 02138, USA
[5] Dipartimento di Fisica e Astronomia, Alma Mater Studiorum, Universit di Bologna, viale Berti Pichat 6/2, I-40127, Bologna, Italy
[6] Department of Physics and Astronomy, University of Southampton, Highfield, SO17 1BJ, UK
[7] INAF-Osservatorio Astronomico di Bologna, Via Ranzani 1, I-40127 Bologna, Italy
[8] Institute for Astronomy, University of Hawaii, 2680 Woodlawn Drive, Honolulu, HI 96822, USA
[9] Max-Planck-Institute für Extraterrestrische Physik, Giessenbachstrasse 1, D-85748 Garching, Germany
[10] Instituto de Astronomia, Universidad Nacional Autonoma de Mexico, Ensenada, Mexico
[11] Institute for Astronomy, Department of Physics, ETH Zurich, Wolfgang-Pauli-Strasse 27, CH-8093 Zurich, Switzerland
[12] University of Hawaii at Hilo, 200 W.Kawili St., Hilo, HI 96720, USA
[13] Argelander-Institut für Astronomie, Universität Bonn, Auf dem Hügel 71, D-53121 Bonn, Germany
Received 2016 May 22; revised 2016 August 2; accepted 2016 August 13; published 2016 November 17

ABSTRACT

We present the measurement of the projected and redshift-space two-point correlation function (2pcf) of the new catalog of *Chandra* COSMOS-Legacy active galactic nucleus (AGN) at $2.9 \leqslant z \leqslant 5.5$ ($\langle L_{\rm bol}\rangle \sim 10^{46}\,{\rm erg\,s^{-1}}$) using the generalized clustering estimator based on phot-z probability distribution functions in addition to any available spec-z. We model the projected 2pcf, estimated using $\pi_{\rm max} = 200\,{\rm h^{-1}\,Mpc}$ with the two-halo term and we derive a bias at $z \sim 3.4$ equal to $b = 6.6^{+0.60}_{-0.55}$, which corresponds to a typical mass of the hosting halos of $\log M_{\rm h} = 12.83^{+0.12}_{-0.11}\,{\rm h^{-1}}\,M_{\odot}$. A similar bias is derived using the redshift-space 2pcf, modeled including the typical phot-z error $\sigma_z = 0.052$ of our sample at $z \geqslant 2.9$. Once we integrate the projected 2pcf up to $\pi_{\rm max} = 200\,{\rm h^{-1}\,Mpc}$, the bias of XMM and *Chandra* COSMOS at $z = 2.8$ used in Allevato et al. is consistent with our results at higher redshifts. The results suggest only a slight increase of the bias factor of COSMOS AGNs at $z \gtrsim 3$ with the typical hosting halo mass of moderate-luminosity AGNs almost constant with redshift and equal to $\log M_{\rm h} = 12.92^{+0.13}_{-0.18}$ at $z = 2.8$ and $\log M_{\rm h} = 12.83^{+0.12}_{-0.11}$ at $z \sim 3.4$, respectively. The observed redshift evolution of the bias of COSMOS AGNs implies that moderate-luminosity AGNs still inhabit group-sized halos at $z \gtrsim 3$, but slightly less massive than observed in different independent studies using X-ray AGNs at $z \leqslant 2$.

Key words: dark matter – galaxies: active – large-scale structure of universe – surveys – X-rays: general

1. INTRODUCTION

The presence of a nuclear supermassive black hole (BH) in almost all galaxies in the present day universe is an accepted paradigm in astronomy (e.g., Kormendy & Richstone 1995; Kormendy & Bender 2011). Despite major observational and theoretical efforts over the last two decades, a clear explanation for the origin and evolution of BHs and their actual role in galaxy evolution remains elusive. Diverse scenarios have been proposed. One possible picture includes a major galaxy merger as the main triggering mechanism (e.g., Menci et al. 2003, 2004; Volonteri et al. 2003; Hopkins et al. 2006). On the other hand, there is mounting observational evidence suggesting that moderate levels of active galactic nucleus (AGN) activity might not be always causally connected to galaxy interactions (Mullaney et al. 2012; Rosario et al. 2013; Villforth et al. 2014). Several works on the morphology of the AGN host galaxies suggest that, even at moderate luminosities, a large fraction of AGNs is not associated with morphologically disturbed galaxies. This trend has been observed both at low ($z \sim 1$, e.g., Georgakakis et al. 2009; Cisternas et al. 2011) and high ($z \sim 2$, e.g., Schawinski et al. 2011, 2012; Kocevski et al. 2012; Treister et al. 2012) redshift. Theoretically, in situ processes, such as disk instabilities or stochastic accretion of gas clouds, have also been invoked as triggers of AGN activity (e.g., Genzel et al. 2008, Dekel et al. 2009; Bournaud et al. 2011).

AGN clustering analysis provides a unique way to unravel the knots of this complex situation, providing important, independent constraints on the BH/galaxy formation and co-evolution. In the cold dark-matter-dominated universe galaxies and their BHs are believed to populate the collapsed dark matter halos, thus reflecting the spatial distribution of dark matter in the universe. The most common statistical estimator for large-scale clustering is the two-point correlation function (2pcf, Davis & Peebles 1983). This quantity measures the excess probability above random to find pairs of galaxies/AGNs separated by a given scale r. By matching the observed 2pcf to detailed outputs of dark matter numerical simulations, one can infer the typical mass of the hosting dark matter halos. This is derived through the so-called AGN bias b, enabling one to pin down the typical environment where AGNs live. This in turn can provide new insights into the physical mechanisms responsible for triggering AGN activity.

The 2pcf of AGNs has been measured in optical large area surveys, such as the 2dF (2QZ, Croom et al. 2005; Porciani &

Norberg 2006) and the Sloan Digital Sky Survey (SDSS, Li et al. 2006; Ross et al. 2009; Shen et al. 2009). These optical surveys are thousands of square degree fields, mainly sampling rare and high luminosity quasars. The amplitude of the 2pcf of quasars suggests that these luminous AGNs are hosted by halos of roughly constant mass, a few times $10^{12}\ M_{\odot}$, out to $z = 3$–4 (Shanks et al. 2011). Models of major mergers between gas-rich galaxies appear to naturally reproduce the clustering properties of optically selected quasars as a function of luminosity and redshift (Hopkins et al. 2007b, 2008; Bonoli et al. 2009; Shen et al. 2009; Shankar et al. 2010). This supports the scenario in which major mergers dominate the luminous quasar population (Scannapieco & Oh 2004; Shankar 2010; Treister et al. 2012; Neistein & Netzer 2014).

Chandra surveys have contributed significantly to the study of the AGN clustering (e.g., CDFS-N, Gilli et al. 2009; *Chandra*/Bootes, Starikova et al. 2011; Allevato et al. 2014). Deep X-ray data can be used to draw conclusions on the faint portions of the AGN luminosity function, where a significant fraction of obscured sources is present. In particular, the *Chandra* survey in the two square degree COSMOS field (C-COSMOS, Elvis et al. 2009; Civano et al. 2012; *Chandra* COSMOS Legacy Survey, Civano et al. 2016) has allowed the investigation of the redshift evolution of the clustering properties of X-ray AGNs, for the first time up to $z \sim 3$. Interestingly, over a broad redshift range ($z \sim 0$–2) moderate-luminosity AGNs occupy DM halo masses of log $M_{\rm h} \sim 12.5$–$13.5\ M_{\odot}\,{\rm h}^{-1}$. The clustering strength of X-ray selected AGNs has been measured by independent studies to be higher than that of optical quasars. Merger models usually fail in reproducing the data from X-ray surveys, opening the possibility of additional AGN triggering mechanisms (e.g., Allevato et al. 2011; Mountrichas & Georgakakis 2012) and/or multiple modes of BH accretion (e.g., Fanidakis et al. 2013). Recently, Mendez et al. (2016) and Gatti et al. (2016) suggested that selection cuts in terms of AGN luminosity, host galaxy properties, and redshift interval, might have a more relevant role in driving the differences often observed in the bias factor inferred from different surveys. The measurement of the AGN bias is crucial at high redshifts, especially at $z > 2$–3, i.e., at the peak in the accretion history of the universe. At $z > 3$, Shen et al. (2007, 2009) measured for the first time the 2pcf of luminous SDSS–DR5 quasars (log $L_{\rm bol} \sim 10^{47}\,{\rm erg\,s^{-1}}$) at $\langle z \rangle = 3.2$ and 3.8. Even if with very large uncertainty, they found that these objects live in massive halos of the order of $10^{13}\ M_{\odot}\,{\rm h}^{-1}$. This result is consistent with models invoking galaxy major mergers as the main triggering mechanism for very luminous AGNs. Recently, Eftekharzadeh et al. (2015) studying a sample of spectroscopically confirmed SDSS-III/BOSS quasars at $2.2 \leqslant z \leqslant 3.4$, performed a more precise estimation of the quasar bias at high redshift. They found no evolution of the bias in three redshift bins, with halo masses equal to $3\times$ and $\sim 0.6 \times 10^{12}\ M_{\odot}\,{\rm h}^{-1}$ at $z \sim 2.3$ and ~ 3, respectively.

There are only a few attempts of measuring the clustering properties of X-ray AGNs at $z \sim 3$. Francke et al. (2008) estimated the bias of a small sample of X-ray AGNs ($L_{\rm bol} \sim 10^{44.8}\,{\rm erg\,s^{-1}}$) in the Extended *Chandra* Deep Field South (ECDFS), with very large uncertainty. They found indications that X-ray ECDFS AGNs reside in dark matter halos with minimum mass of log $M_{\rm min} = 12.6^{+0.5}_{-0.8}\,{\rm h}^{-1}\,M_{\odot}$. On the other hand, Allevato et al. (2014) used a sample of *Chandra* and *XMM-Newton* AGNs in COSMOS with moderate-luminosity (log $L_{\rm bol} \sim 10^{45.3}\,{\rm erg\,s^{-1}}$) at $\langle z \rangle = 2.86$. For the first time, they estimated the bias of X-ray selected AGNs at high redshift, suggesting that they inhabit halos of log $M_{\rm h} = 12.37 \pm 0.10\ M_{\odot}\,{\rm h}^{-1}$. They also extended to $z \sim 3$ the result that Type 1 AGNs reside in more massive halos than Type 2 AGNs. Recently, Ikeda et al. (2015) estimated the clustering properties of low-luminosity quasars in COSMOS at $3.1 \leqslant z \leqslant 4.5$, using the cross-correlation between Lyman-Break Galaxies (LBGs) and 25 quasars with spectroscopic and photometric redshifts. They derived an 86% upper limit of 5.63 for the bias at $z \sim 4$.

In this paper, we want to extend the study of the clustering properties of X-ray selected AGNs to $z > 3$ using the new *Chandra* COSMOS-Legacy data. To this goal, we perform clustering measurements using techniques based on photometric redshift in the form of probability distribution functions (Pdfs), in addition to any available spectroscopy. This is motivated by the development in the last years of clustering measurement techniques based on photometric redshift Pdfs by Myers et al. (2009), Hickox et al. (2011, 2012), Mountrichas et al. (2013), and Georgakakis et al. (2014). One of the advantages of this new clustering estimator is that one can use in the analysis all sources not just the optically brighter ones for which spectroscopy is available. For this reason, it is well suited to clustering investigations using future large X-ray AGN surveys, where the fraction of spectroscopic redshifts might be small.

Throughout the paper, all distances are measured in comoving coordinates and are given in units of Mpc h^{-1}, where $h = H_0/100\ {\rm km\,s^{-1}}$. We use a ΛCDM cosmology with $\Omega_M = 0.3$, $\Omega_{\Lambda} = 0.7$, $\Omega_b = 0.045$, and $\sigma_8 = 0.8$. The symbol log signifies a base-10 logarithm.

2. AGN SAMPLE AT $2.9 \leqslant z \leqslant 5.5$

The *Chandra*-COSMOS-Legacy survey (CCLS) is the combination of the 1.8 Ms C-COSMOS survey (Elvis et al. 2009) with 2.8 Ms of new *Chandra* ACIS-I observations (Civano et al. 2016) for a total coverage of $2.2\,{\rm deg}^2$ of the COSMOS field (Scoville et al. 2007). The X-ray source catalog consists of 4016 sources. 2076 (∼52%) have a secure spectroscopic redshift (spec-z) and for ∼96% the photometric redshift (photo-z) is available. As shown in Marchesi et al. (2016a), the spectroscopic redshifts have been obtained with different observing programs, such as the zCOSMOS survey (Very Large Telescope/VIMOS; Lilly et al. 2007) and the *Magellan*/IMACS survey (Trump et al. 2007, 2009). Other programs, many of which have been specifically targeting the CCLS have been carried out with Keck-MOSFIRE (P.I. F. Civano, N. Scoville), Keck-DEIMOS (P.I.s Capak, Kartaltepe, Salvato, Sanders, Scoville, Hasinger), Subaru- FMOS (P.I. J. Silverman), VLT-FORS2 (P.I. J. Coparat), and *Magellan*-PRIMUS (public data).

The photo-zs are estimated following the procedure described in Salvato et al. (2011). Following Marchesi et al. (2016b), the accuracy of the photometric redshifts with respect to the whole spectroscopic redshift sample is $\sigma_{\Delta z/(1+z_{\rm spec})} = 0.02$, with a fraction of outliers ≃11%. At $z > 2.9$, there are nine outliers ($\Delta z/(1 + z_{\rm spec}) > 0.15$), but for the remaining sources the agreement between spec-z and photo-z has the same quality of the whole sample. In detail, the normalized

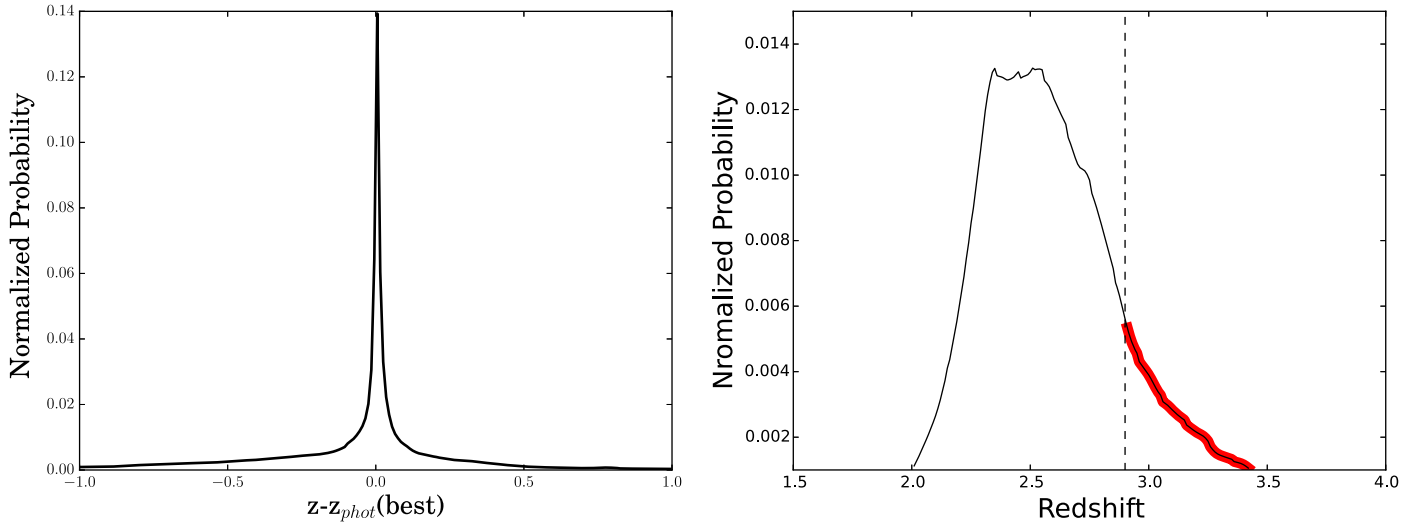

Figure 1. Left panel: mean normalized phot-z Pdf of all CCL AGNs with best-fit phot-$z > 2.9$. Right panel: normalized phot-z Pdf for the source lid766. This source has a best-fit photo-z value <2.9, but a phot-z Pdf($z_i > 2.9$)>0.001 (red thick line). The redshifts above this threshold, weighted by their Pdf, have been taken in account in the catalog used to estimate the 2pcf.

median absolute deviation $\sigma_{\rm NMAD} = 1.48 \times$ median ($\|z{\rm spec} - z{\rm phot}\|/(1 + z{\rm spec})) = 0.012$.

The CCL AGN sample at $2.9 < z < 5.5$ consists of 212 AGNs detected in the 0.5–10 keV band, 107/212 with spec-zs and 105/212 with only phot-zs. To each of the 105 AGNs with best-fit phot-z in the range of $2.9 \leqslant z < 5.5$, is associated a probability distribution function (Pdf), which gives the probability of the source to be in the redshift range of $z_i \pm \Delta\, z/2$ with a binsize of $\Delta z = 0.01$. The integrated area of the Pdf on all redshift bins z_i is normalized to one, i.e., $\sum_i {\rm Pdf}(z_i) = 1$ for each AGN. We take into account for this analysis the redshift bins z_i with ${\rm Pdf}(z_i) > 0.001$. Figure 1 shows the mean normalized phot-z Pdf for 105 sources with best-fit phot-z $2.9 \leqslant z < 5.5$. The effective contribution to the number of AGNs at $z \geqslant 2.9$ of these 105 AGNs weighted by the Pdf is 78.32 sources, i.e., $\sum_{j=1}^{105} {\rm Pdf}_j(z \geqslant 2.9) = 78.32$.

In the CCL sample, there are also 246 sources with phot-z < 2.9 but that contribute to the Pdf at $2.9 \leqslant z \leqslant 5.5$ (i.e., with Pdf > 0.001 at $2.9 \leqslant z_i \leqslant 5.5$; see for example the Pdf of source lid766, whose nominal best-fit phot-z value is 2.51, in Figure 1). All of these 246 sources have been taken in account in our analysis, using for each of them the Pdf of each bin of redshift $2.9 \leqslant z_i \leqslant 5.5$. The weighted contribution of these sources, i.e., the sum of all weights, is equal to 36.3 AGNs ($\sum_{j=1}^{246} {\rm Pdf}_j(z \geqslant 2.9) = 36.3$). To all the 107 sources with known spec-z, we assign a ${\rm Pdf}_j = 1$ to the spec-z value ($\sum_{j=1}^{107} {\rm Pdf}_j = 107$). To summarize, the total effective number of CCL AGNs at $2.9 \leqslant z < 5.5$ weighted by the Pdf and used for the clustering measurements is $78.3 + 36.3 + 107 = 221.6$ objects.

Figure 2 shows the normalized redshift and 2–10 keV rest-frame X-ray luminosity distribution for our sample of CCL AGN at $2.9 < z < 5.5$, when the phot-z Pdfs are used (black dotted line, $\langle z \rangle = 3.36$). The mean bolometric luminosity of this sample derived using the bolometric correction defined in Equation (21) of Marconi et al. (2004) is $\log \langle L_{\rm bol} \rangle = 45.99\ {\rm erg\ s^{-1}}$. For comparison, we also show the normalized distributions of our AGN sample when only the best-fit phot-zs are taken into account in addition to any available spec-z (gray solid line, $\langle z \rangle = 3.34$) and for the sample with known spec-z (red-dashed line, $\langle z \rangle = 3.35$).

3. 2PCF USING PHOT-Z PDFS

3.1. Projected 2pcf

The most commonly used quantitative measure of large-scale structure is the 2pcf, $\xi(r)$, which traces the amplitude of AGN clustering as a function of scale. $\xi(r)$ is defined as a measure of the excess probability dP, above what is expected for an unclustered random Poisson distribution, of finding an AGN in a volume element dV at a separation r from another AGN:

$$dP = n[1 + \xi(r)]dV, \tag{1}$$

where n is the mean number density of the AGN sample (Peebles 1980). Measurements of $\xi(r)$ are generally performed in comoving space, with r having units of $\rm h^{-1}$ Mpc.

With a redshift survey, we cannot directly measure $\xi(r)$ in physical space, because peculiar motions of galaxies distort the line-of-sight distances inferred from redshift. To separate the effects of redshift distortions, the spatial correlation function is measured in two-dimensions $r_{\rm p}$ and π, where $r_{\rm p}$ and π are the projected comoving separations between the considered objects in the directions perpendicular and parallel, respectively, to the mean line of sight between the two sources. Following Davis & Peebles (1983), r_1 and r_2 are the redshift positions of a pair of objects, s is the redshift-space separation $(r_1 - r_2)$, and $l = \frac{1}{2}(r_1 + r_2)$ is the mean distance to the pair. The separations between the two considered objects across $r_{\rm p}$ and π are defined as

$$\pi = \frac{\boldsymbol{s} \cdot \boldsymbol{l}}{|\boldsymbol{l}|} \tag{2}$$

$$r_{\rm p} = \sqrt{(\boldsymbol{s} \cdot \boldsymbol{s} - \pi^2)}. \tag{3}$$

Redshift-space distortions only affect the correlation function along the line of sight, so we estimate the so-called projected

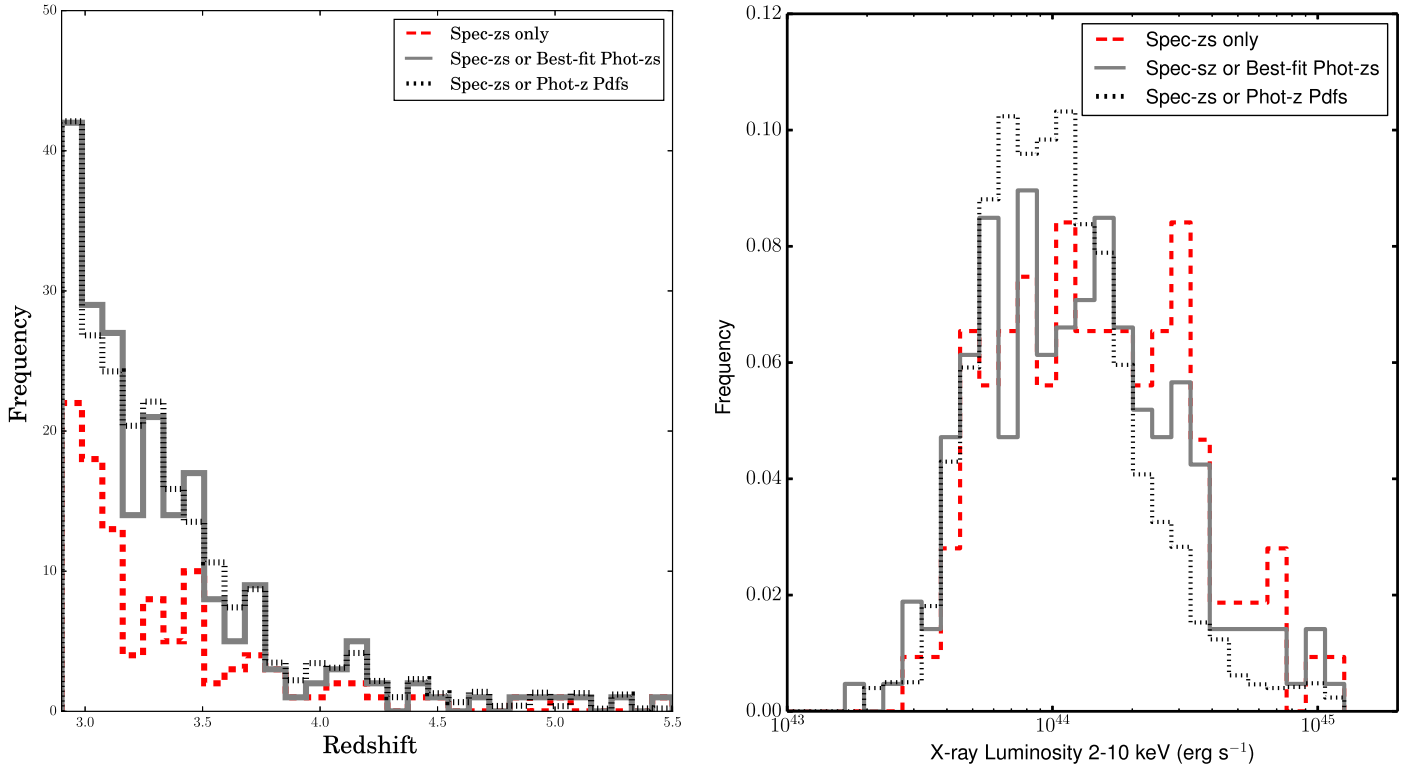

Figure 2. Redshift (left panel) and 2–10 keV X-ray luminosity (right panel) distribution for 107 CCL AGNs with known spec-z (red-dashed line), 212 AGNs with known spec or best phot-z (solid gray line), and 221.6 AGNs with known spec-z or phot-z weighted by the Pdf (black dotted line), at $2.9 \leqslant z \leqslant 5.5$

correlation function $w_{\rm p}(r_{\rm p})$ (Davis & Peebles 1983):

$$w(\sigma) = 2\int_0^{\pi_{\rm max}} \xi(\sigma, \pi) d\pi, \quad (4)$$

where $\xi(r_{\rm p}, \pi)$ is the 2pcf in terms of $r_{\rm p}$ and π, measured using the Landy & Szalay (1993, LS) estimator:

$$\xi = \frac{1}{\rm RR'}[{\rm DD'} - 2{\rm DR'} + {\rm RR'}], \quad (5)$$

where DD', DR', and RR' are the normalized data–data, data–random, and random–random pairs.

In this classic approach of estimating the redshift-space correlation function, in the presence of accurate spec-zs, when a data–data pair with separation $(r_{\rm p}, \pi)$ is found, the pair number is incremented by one, i.e., ${\rm DD}(r_{\rm p}, \pi) = {\rm DD}(r_{\rm p}, \pi) + 1$. Following Georgakakis et al. (2014), in the generalized clustering estimator the number of data–data pairs with projected and line-of-sight separation $(r_{\rm p}, \pi)$ is, instead, incremented by the product ${\rm Pdf}_1(z_i) \times {\rm Pdf}_2(z_j)$:

$${\rm DD}(r_{\rm p}, \pi) = {\rm DD}(r_{\rm p}, \pi) + {\rm Pdf}_1(z_i) \times {\rm Pdf}_2(z_j), \quad (6)$$

where ${\rm Pdf}_1(z_i)$ and ${\rm Pdf}_2(z_j)$ are the Pdf values (per redshift bin) of the source 1 at $z = z_i$ and of the source 2 at $z = z_j$ respectively.

The measurements of the 2pcf requires the construction of a random catalog with the same selection criteria and observational effects as the data. To this end, we constructed a random catalog, where each simulated source is placed at a random position in the sky, with its flux randomly extracted from the catalog of real source fluxes. The simulated source is kept in the random sample if its flux is above the sensitivity map value at that random position (Miyaji et al. 2007; Cappelluti et al. 2009). The corresponding redshift for each random object is then assigned based on the smoothed redshift distribution of the AGN sample, where each redshift is weighted by the Pdf associated to that redshift for the particular source. Since the phot-z Pdfs are already taken into account in the generation of the random redshifts, we decided to assign Pdf = 1 to each random source.

In the halo model approach, the large-scale amplitude signal is due to the correlation between objects in distinct halos and the bias parameter defines the relation between the large-scale clustering amplitude of the AGN correlation function and the DM 2-halo term:

$$b^{2-h}(r_{\rm p}) = (w_{\rm AGN}(r_{\rm p}) / w_{\rm DM}^{2-h}(r_{\rm p}))^{1/2}. \quad (7)$$

We first estimated the DM 2-halo term at the median redshift of the sample, using

$$w_{\rm DM}^{2-h}(r_{\rm p}) = 2\int_{r_{\rm p}}^{\infty} \frac{\xi_{\rm DM}^{2-h}(r) r dr}{\sqrt{r^2 - r_{\rm p}^2}} \quad (8)$$

integrating up to $r_{\rm max} = 200\,{\rm h}^{-1}\,{\rm Mpc}$, where

$$\xi_{\rm DM}^{2-h}(r) = \frac{1}{2\pi^2}\int P^{2-h}(k) k^2 \left[\frac{\sin(kr)}{kr}\right] dk. \quad (9)$$

$P^{2-h}(k)$ is the linear power spectrum, assuming a power spectrum shape parameter $\Gamma = \Omega_m h = 0.2$ (Efstathiou et al. 1992) that corresponds to $h = 0.7$.

3.2. z-Space Correlation Function

Similarly, we can estimate the z-space correlation function $\xi(s)$ using Equations (5) and (6) written now as a function of

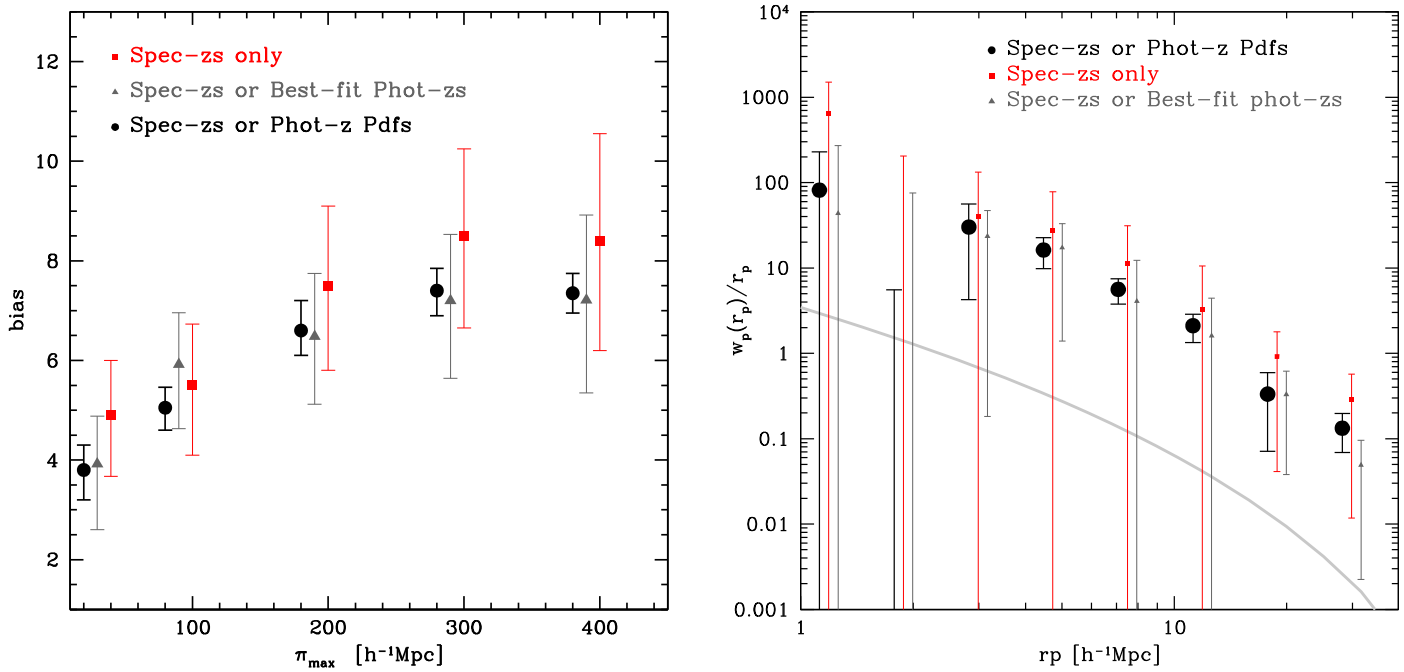

Figure 3. Left panel: bias as a function of π_{max} for 221.6 CCL AGNs at $2.9 \leqslant z < 5.5$, when the projected 2pcf is measured using the generalized clustering estimator based on phot-z Pdfs in addition to any available spec-z (black dots). For comparison, the gray triangles and red squares show the bias of 212 AGNs with known spec or best-fit phot-z and 107 AGNs with known spec-zs at $2.9 < z < 5.5$ when the classic LS estimator (i.e., no phot-z Pdfs) is used. Right panel: projected 2pcf for $\pi_{max} = 200\ h^{-1}$ Mpc. The 1σ errors on $w_p(r_p)$ are the square root of the diagonal components of the covariance matrix. The continuous line represents the DM projected 2pcf estimated at $\langle z \rangle = 3.36$.

the redshift-space separation $s = (r_1 - r_2)$ between the sources. $\xi(s)$ is affected by perturbations in the cosmological redshifts due to peculiar velocities and redshift errors. The z-space power spectrum can be modeled in polar coordinates as follows (e.g., Kaiser 1987; Peacock et al. 2001).

$$P(k, \mu) = P_{DM}(k)(b + f\mu^2)^2 \exp(-k^2\mu^2\sigma^2), \quad (10)$$

where $k = \sqrt{k_\perp^2 + k_\parallel^2}$, $k_\perp$ and $k_\parallel$ are the wavevector components perpendicular and parallel to the line of sight, respectively. $\mu = k_\perp/k_\parallel$, $P_{DM}(k)$ is the dark matter power spectrum, b is the linear bias factor, and f is the growth rate of density fluctuations. σ is the displacement along the line of sight due to random perturbations of cosmological redshifts. Assuming standard gravity, we approximated the growth rate $f \simeq \Omega_M(z)^\gamma$, with $\gamma = 0.545$ (e.g., Sereno et al. 2015).

The $f\mu^2$ term parametrizes the coherent motions due to large-scale structures, enhancing the clustering signal on all scales. The exponential cut-off term describes the random perturbations of the redshifts caused by both nonlinear stochastic motions and redshift errors. The integration of Equation (7) over the angle μ, and then the Fourier anti-transformation gives

$$\xi(s) = b^2\xi'(s) + b\xi''(s) + \xi'''(s). \quad (11)$$

The main term, $\xi'(s)$, is the Fourier anti-transform of the monopole $P'(k)$:

$$P'(k) = P_{DM}(k)\frac{\sqrt{\pi}}{2k\sigma} erf(k\sigma), \quad (12)$$

that corresponds to the model given by Equation (10) when neglecting the dynamic distortion term.

In our case, photo-z errors perturb the most the distance measurements along the line of sight. Therefore, the small-scale random motions are negligible with respect to photo-z errors. The cut-off scale in Equation (12) can thus be written as

$$\sigma = \frac{c\sigma_z}{H(z)}, \quad (13)$$

where H(z) is the Hubble function computed at the median redshift of the sample, and σ_z is the typical photo-z error.

In this case, knowing the cut-off scale, the AGN bias can be derived from the Fourier anti-transform of the monopole $P'(k)$, i.e.,

$$b^2 = \frac{\xi'(s)}{\xi(s)}, \quad (14)$$

where $\xi(s)$ is the observed z-space 2pcf of our AGN sample.

4. RESULTS

4.1. $w_p(r_p)$ and Bias

We have measured the 2pcf of 221.6 CCL AGNs at $2.9 \leqslant z < 5.5$, using the generalized clustering estimator defined in Equation (6), based on phot-z Pdfs in addition to any available spec-z. The projected 2pcf $w_p(r_p)$ is then estimated using Equation (4).

The typical value of π_{max} used in clustering measurements of both optically selected luminous quasars and X-ray selected AGNs is ~20–100 h^{-1} Mpc (e.g., Zehavi et al. 2005; Coil et al. 2009; Krumpe et al. 2010; Allevato et al. 2011). The optimum π_{max} value can be determined by measuring the 2pcf for different π_{max} and then adopting the value at which the amplitude of the signal appears to level off.

Figure 3 (left panel) shows the bias factor estimated for different values of π_{max} in Equation (4), when the phot-z Pdfs are used in addition to any available spec-z. For comparison,

Table 1
Properties of the AGN Samples

Sample	N	$\Sigma \mathrm{Pdf}_j(z \geqslant 2.9)$	$\langle z \rangle$	$\log \langle L_{\mathrm{bol}} \rangle$ erg s^{-1}	b Equation (7)	$\log M_{\mathrm{h}}$ $\mathrm{h}^{-1}\,\mathrm{M}_{\odot}$	b Equation (14)	$\log M_{\mathrm{h}}$ $\mathrm{h}^{-1}\,\mathrm{M}_{\odot}$
Spec-zs + Phot-z Pdfs	457	221.6	3.36[a]	45.99 ± 0.53	$6.6^{+0.6}_{-0.55}$	$12.83^{+0.12}_{-0.11}$	$6.53^{+0.52}_{-0.55}$	$12.82^{+0.11}_{-0.13}$
Spec-zs + Best-fit Phot-zs	212	212	3.34	45.93 ± 0.17	$6.48^{+1.27}_{-1.36}$	$12.81^{+0.24}_{-0.35}$	$6.96^{+0.72}_{-0.73}$	$12.90^{+0.15}_{-0.15}$
Spec-zs only	107	107	3.35	45.92 ± 0.34	$7.5^{+1.6}_{-1.7}$	$13.0^{+0.25}_{-0.35}$	$7.98^{+1.4}_{-1.5}$	$13.08^{+0.22}_{-0.25}$

Note.
[a] Mean redshift of the sample weighted by the Pdfs.

we also estimated the bias for case (i) 107 AGNs with known spec-zs; case (ii) 107 + 105 AGNs with known spec-z or best-fit phot-zs. In these cases, the 2pcf is measured using the classic LS estimator and the Pdf is set to unity for each source.

As expected, when including phot-zs in the analysis, the bias levels-off only at large scales, because of the large uncertainties in the redshifts measured via photometric methods (Georgakakis et al. 2014). Surprisingly, even if the error bars are large, an increase of the bias factor at $\pi_{\mathrm{max}} > 100\,\mathrm{h}^{-1}$ Mpc is suggested also when only spec-zs are used with the classic 2pcf estimator. This suggests that a fraction of spec-zs might be affected by large errors (see Section 4.2).

The amplitude of the projected 2pcf of CCL AGNs measured using the generalized clustering estimator converges at $\pi_{\mathrm{max}} \geqslant 200\,\mathrm{h}^{-1}$ Mpc. We decide to use $\pi_{\mathrm{max}} = 200\,\mathrm{h}^{-1}$ Mpc in order to balance the advantage of integrating out redshift-space distortions against the disadvantage of introducing noise from uncorrelated line-of-sight structure.

Figure 3 (right panel) shows the projected 2pcf estimated using the generalized clustering estimator, with $\pi_{\mathrm{max}} = 200\,\mathrm{h}^{-1}$ Mpc. The 1σ errors on $w_{\mathrm{p}}(r_{\mathrm{p}})$ are the square root of the diagonal components of the covariance matrix (Miyaji et al. 2007; Krumpe et al. 2010) estimated using the bootstrap method. The latter quantifies the level of correlation between different bins. For comparison, we also estimate the projected 2pcf for case (i) 107 AGNs with known spec-zs; case (ii) 107 + 105 AGNs with known spec-z or best-fit phot-zs. Note that, in these cases, the classic LS estimator is used (i.e., Pdf = 1 for each source) and π_{max} is fixed to $200\,\mathrm{h}^{-1}$ Mpc also in these cases.

Following Equation (7), we derive the best-fit bias by using a χ^2 minimization technique with one free parameter in the range of $r_{\mathrm{p}} = 1$–$30\,\mathrm{h}^{-1}$ Mpc, where $\chi^2 = \Delta^{\mathrm{T}} M_{\mathrm{cov}}^{-1} \Delta$. In detail, Δ is a vector composed of $w_{\mathrm{p}}(r_{\mathrm{p}}) - w_{\mathrm{mod}}(r_{\mathrm{p}})$ (see Equations (4) and (7)), Δ^{T} is its transpose and M_{cov}^{-1} is the inverse of covariance matrix. The latter full covariance matrix is used in the fit to take into account the correlation between errors.

As shown in Table 1, we derived a bias for our sample of CCL AGNs equal to $b = 6.6^{+0.60}_{-0.55}$ at $\langle z \rangle = 3.36$. Following the bias-mass relation $b(M_{\mathrm{h}}, z)$ described in van den Bosch (2002) and Sheth et al. (2001), the AGN bias corresponds to a typical mass of the hosting halos of $\log M_{\mathrm{h}} = 12.83^{+0.12}_{-0.11}\,\mathrm{h}^{-1}\,M_{\odot}$. It is worth noticing that this is a typical/characteristic mass of the halos hosting CCL AGNs. Only the HOD modeling of the clustering signal at all scales can provide the entire hosting halo mass distribution for this sample.

The bias has a larger uncertainty when derived from the 2pcf estimated without the phot-z Pdfs. In detail, we find $b = 7.5^{+1.6}_{-1.7}$ at $\langle z \rangle = 3.35$ for 107 AGNs with known spec-zs (case (i)) and $b = 6.48^{+1.27}_{-1.36}$ at $\langle z \rangle = 3.34$ for 107 + 105 AGNs with known spec or best-fit phot-zs (case (ii)). Note that in these cases the 2pcf is measured using the classic LS estimator and the Pdf is set to unity for each source.

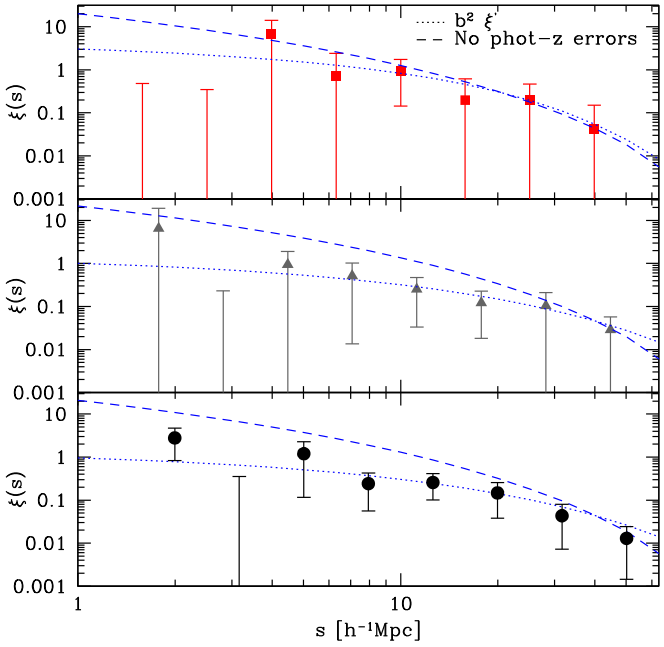

Figure 4. Redshift-space correlation function of 221.6 CCL AGNs at $2.9 < z < 5.5$ derived using the generalized clustering estimator based on phot-z Pdfs in addition to any available spec-z (black circles in the bottom panel). For comparison, the gray triangles (middle panel) and the red squares (upper panel) show the 2pcf of 212 AGNs with known spec or best-fit phot-z and 107 AGNs with known spec-zs at $2.9 < z < 5.5$ estimated using the classic LS estimator (i.e., Pdf = 1 for each source). The dotted lines show the best-fit models obtained including the dominant term $b^2\xi'$ in Equation (11), while the dashed lines is the model without the photo-z damping term. The error bars show the square roots of the diagonal values of the covariance matrix.

4.2. $\xi(s)$ and Phot-z Errors

To investigate the effect of phot-z errors on the 2pcf, we also measured the z-space correlation function $\xi(s)$. Figure 4 shows $\xi(s)$ for 221.6 CCL AGNs using the generalized clustering estimator based on phot-z Pdfs in addition to any available spec-z. For comparison, the gray triangles show $\xi(s)$ for cases (1) and (2).

As described in Section 3.2, $\xi(s)$ is affected by the Kaiser effect that enhances the clustering signal at all scales and by phot-z errors, that are modeled by using an exponential cut-off in the z-space power spectrum. For our sample of CCL AGNs, the typical error on phot-zs is $\sigma_z = 0.012 \times (1 + z_{\mathrm{spec}}) = 0.052$ at $\langle z \rangle = 3.4$. This implies a cut-off scale

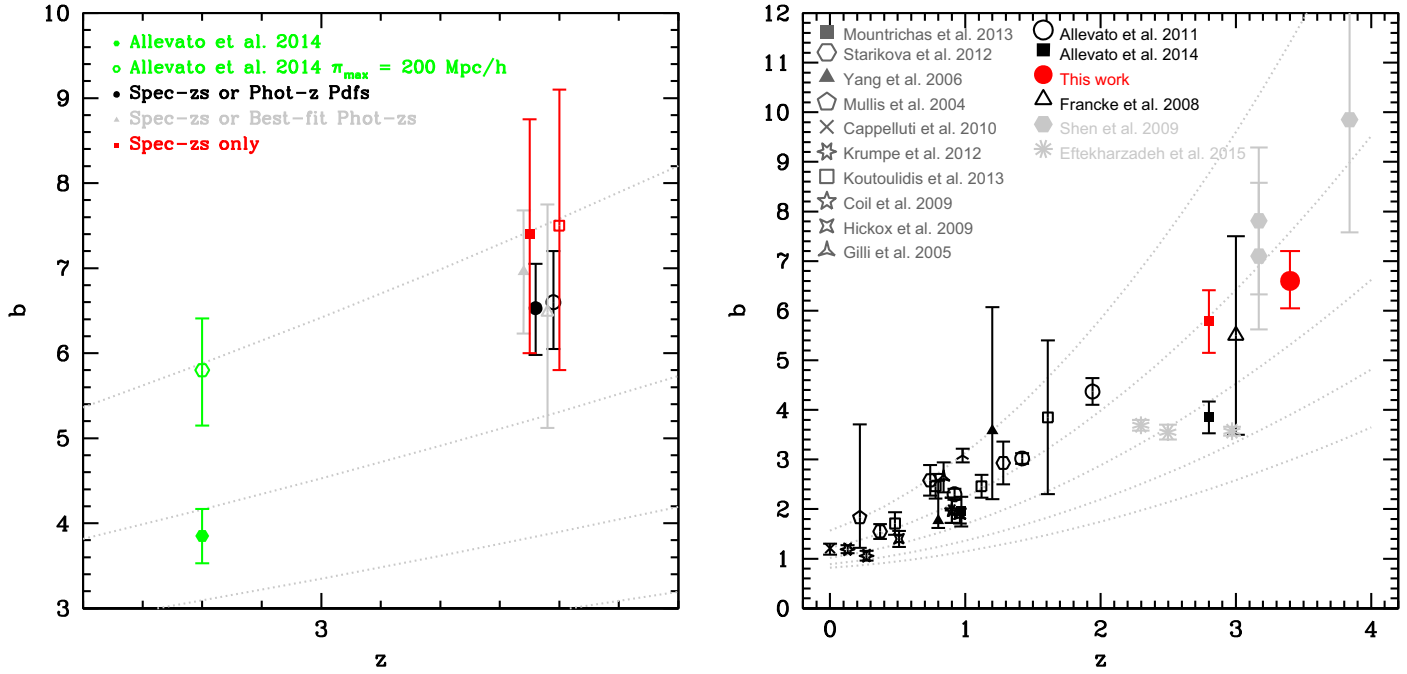

Figure 5. Left panel: bias of CCL AGNs at $z \sim 3.4$ estimated using the projected 2pcf (empty points) and the z-space 2pcf (filled points). The empty symbols are offset in the horizontal direction by +0.04 for clarity. For comparison, the bias of XMM and *Chandra* COSMOS AGNs at $z = 2.8$ is shown as presented in Allevato et al. (2014) using $\pi_{\rm max} = 40\,h^{-1}$ Mpc (filled hexagon) and when the bias is re-estimated using $\pi_{\rm max} = 200\,h^{-1}$ Mpc. The dashed lines show the expected b(z) of typical DM halo with mass of 12, 12.5, and 13 $h^{-1}\,M_{\odot}$ in log scale (from bottom to top), based on Sheth et al. (2001) formalism. Right panel: bias parameter as a function of redshift for X-ray selected AGNs (black) from previous studies as described in the legend. The red circle at $z \sim 3.4$ show the bias factors as estimated in this work for CCL AGNs. The red square shows the bias factor as re-estimated in the present paper using the same catalog of XMM and *Chandra*-COSMOS AGNs used in Allevato et al. (2014), but with $\pi_{\rm max} = 200\,h^{-1}$ Mpc. The dashed lines show the expected b(z) of typical DM halo with masses of 11.5, 12, 12.5, 13, and 13.5 $h^{-1}\,M_{\odot}$ in log scale (from bottom to top), based on Sheth et al. (2001). Bias factors from different studies (Gilli et al. 2005; Hickox et al. 2009; Koutoulidis et al. 2013) are converted to a common cosmology ($\Omega_{\Lambda} = 0.7$, $\Omega_m = 0.3$, $\sigma_8 = 0.8$).

$\sigma = 43.45\,h^{-1}$ Mpc (see Equation (13)). Including the phot-z damping in the modeling of $\xi(s)$, we derived the best-fit bias by using Equation (14) and the χ^2 minimization technique with one free parameter in the range of $s = 1$–$50\,h^{-1}$ Mpc. In particular, for the z-space 2pcf measured using the generalized clustering estimator, we derived $b = 6.53^{+0.52}_{-0.58}$. For the sample of 212 AGNs with known spec or best-fit phot-zs for which the classic clustering estimator is used, we derived $b = 6.96^{+0.72}_{-0.73}$. These values are in perfect agreement with the bias obtained from the projected 2pcf with $\pi_{\rm max} = 200\,h^{-1}$ Mpc. This confirms that the convergence of the projected 2pcf observed only at large scales ($\pi_{\rm max} \geqslant 200\,h^{-1}$ Mpc) is due to large phot-z errors. In fact, for large redshift errors and small survey area, it is necessary to integrate the correlation function up to large scales to fully correct for them.

We also estimated the bias using the z-space 2pcf for 107 AGNs with known spec-zs. In general, we do not expect spec-zs to be affected by large errors. If we do not include the phot-z damping in the model of $\xi(s)$, we obtain for this sample a bias $b = 5.86^{+1.13}_{-1.05}$, which is lower than $b = 7.5^{+1.6}_{-1.7}$ obtained using the projected 2pcf and $\pi_{\rm max} = 200\,h^{-1}$ Mpc. A better fit of $\xi(s)$ and a larger bias can be obtained only if we include in the model spec-z errors of the order of $\sigma_z = 0.02$–0.025. In particular, for $\sigma_z = 0.020$ (cut-off scale $\sigma = 16.7\,h^{-1}$ Mpc) and $\sigma_z = 0.025$ ($\sigma = 20.9\,h^{-1}$ Mpc), we derived $b = 7.4^{+1.35}_{-1.40}$ and $b = 8.01^{+1.4}_{-1.5}$, respectively. However, given the low statistics, smaller values of σ_z and then of the bias cannot be ruled-out. This error redshift is larger than what is expected for a spectroscopic sample of AGNs. However, the presence in the spectroscopic sample of ~20% of the objects (21/107) with a low quality flag (i.e., flag = 1.5, corresponding to low quality spectra, and therefore not fully reliable redshift, but with known phot-z such that $\sigma_{\Delta z/(1+z_{\rm spec})} < 0.1$) could explain both the improvement of the fit including such an error in the analysis and the increase of the bias with increasing $\pi_{\rm max}$ up to $\sim 200\,h^{-1}$ Mpc when using only AGNs with spectroscopic redshift.

5. DISCUSSION

In this section, we compare our results with previous measurements using COSMOS AGNs at $z \sim 3$ and with previous studies at similar redshift. We also interpret our results in terms of AGN triggering mechanisms.

5.1. Redshift Evolution of the AGN Bias

Figure 5 (right panel) shows the redshift evolution of the AGN bias estimated using moderate-luminosity AGNs detected in different X-ray surveys. Interestingly, moderate-luminosity AGNs occupy DM halo masses of $\log M_{\rm h} \sim 12.5$–$13.5\,M_{\odot}\,h^{-1}$ up to $z \sim 2$, tracing a constant group-sized halo mass. Allevato et al. (2011) have shown that XMM-COSMOS AGNs ($L_{\rm bol} \sim 10^{45.2}$ erg s^{-1}) reside in DM halos with constant mass equal to $\log M_{\rm h} = 13.12 \pm 0.07\,M_{\odot}\,h^{-1}$ up to $z = 2$. They also argue that this high bias cannot be reproduced assuming that major merger between gas-rich galaxies (Shen et al. 2009) is the main triggering scenario for moderate-luminosity AGNs. By contrast, at $z \sim 3$, Allevato et al. (2014) found a drop in the mass of the hosting halos, with *Chandra* and *XMM-Newton* COSMOS AGNs ($L_{\rm bol} \sim 10^{45.3}$ erg s^{-1}), inhabiting halos of $\log M_{\rm h} = 12.37 \pm 0.10\,M_{\odot}\,h^{-1}$.

In the present paper, we measure a bias for 221.6 CCL AGNs at $2.9 \leqslant z \leqslant 5.5$ equal to $b = 6.6^{+0.6}_{-0.55}$, that corresponds to a typical mass of the hosting dark matter halos of log $M_{\rm h} = 12.83^{+0.12}_{-0.11}$ $h^{-1} M_{\odot}$. This result suggests a higher bias for CCL AGNs compared to previous studies in the COSMOS at $z \sim 3$. In fact, Allevato et al. (2014) found a bias of $3.85^{+0.22}_{-0.21}$ at $\langle z \rangle = 2.8$, using a sample of XMM and *Chandra* AGNs. Although the two samples only partially overlap, we argue that the most likely explanation of these differences lies in the small value of $\pi_{\rm max}$ ($= 40\,h^{-1}$ Mpc) used in Allevato et al. (2014). As shown in Figure 3, the bias strongly increases with $\pi_{\rm max}$ due to the large phot-z errors and the use of $40\,h^{-1}$ Mpc might produce an underestimated clustering signal.

To verify this effect, we took the same sample used in Allevato et al. (2014), i.e., 346 XMM and *Chandra* COSMOS AGN with known spec or phot-$z > 2.2$. As already mentioned, Allevato et al. (2014) used the classic LS estimator where the phot-zs Pdfs are not taken into account. Using their same classic approach, we estimated the projected 2pcf for different values of $\pi_{\rm max}$ and found that the clustering signal converges only at $\pi_{\rm max} \geqslant 200\,h^{-1}$ Mpc. In particular, we derived a bias $b = 5.8^{+0.61}_{-0.65}$ for $\pi_{\rm max} = 200\,h^{-1}$ Mpc, which corresponds to a typical hosting halo mass log $M_{\rm h} = 12.92^{+0.13}_{-0.18}$. As shown in Figure 5 (left panel), the bias estimated using $\pi_{\rm max} = 200\,h^{-1}$ Mpc is in agreement with the bias of CCL AGNs at $z \sim 3.4$ as derived in the present work. It is worth noticing that the mean luminosity of the samples is also increasing with z, with mean $L_{\rm bol} = 10^{45.5}$ erg s^{-1} for XMM and *Chandra* COSMOS AGNs at $z \sim 3$ and $\sim$46 erg s^{-1} for CCL AGNs at higher z.

These results imply that at $z > 3$: (i) the typical hosting halo mass of moderate-luminosity AGNs remains almost constant with redshift, going from $\sim 8.3 \times 10^{12}$ at $z = 2.8$ to $\sim 6.7 \times 10^{12}\,M_{\odot}\,h^{-1}$ at $z \sim 3.4$, since a lower mass is required to yield the same bias at a higher redshift; (ii) moderate-luminosity AGNs still inhabit group-sized halos at high redshift, but slightly less massive than observed in different independent studies using X-ray selected AGNs at $z \leqslant 2$.

5.2. Previous Studies at High Redshift

The evolution of the bias with redshit has been studied in Eftekharzadeh et al. (2015) for SDSS-III/BOSS quasars at $2.2 \leqslant z \leqslant 3.4$. They investigated the redshift dependence of quasar clustering in three redshift bins and found no evolution of the correlation length and bias. In terms of halo mass, this corresponds to a characteristic halo mass that decreases with redshift, with halo masses of $3 \times (6\times)$ and $\sim 0.6 \times (1.3\times)\ 10^{12}\,M_{\odot}\,h^{-1}$ at $z \sim 2.3$ and ~ 3, respectively, where the dark matter halo masses are estimated using Tinker et al. (2010; Sheth et al. 2001).

These results are surprisingly different in terms of bias and halo mass when compared to Shen et al. (2009). At $z \sim 3$, Eftekharzadeh et al. (2015) derived halo masses that are close to an order-of-magnitude smaller than those presented in Shen et al. (2009). In this latter study, they measured the bias of SDSS-DR5 quasars with mean $L_{\rm bol} \sim 10^{47}$ erg s^{-1}, at $\langle z \rangle = 3.2$. Even if with large uncertainties, their results suggest that luminous quasars reside in massive halos with masses that are a few times $10^{13}\,h^{-1}\,M_{\odot}$ (based on Sheth et al. 2001). Although the two samples do not completely overlap, Eftekharzadeh et al. (2015) argue that the most likely explanation of these differences lies in the improvements in SDSS photometric calibration and target selection algorithms as well as in the much larger number of quasars that afford greater measurements precision compared to Shen et al. (2009).

Our results are in disagreement with the bias factor equal to $b = 3.57 \pm 0.09$ at $z \sim 3$, derived in Eftekharzadeh et al. (2015). This disagreement might be due to the slightly different average redshift and the significantly different luminosity (almost one order of magnitude) of the samples used in the two different studies. An additional important difference between the samples is that our catalog of CCL AGNs includes both Type 1 and Type 2 AGNs, while Eftekharzadeh et al. (2015) use Type 1 BOSS luminous quasars. It is also worth noticing that in Eftekharzadeh et al. (2015) the bias is derived modeling the z-space 2pcf in the Kaiser formalism, i.e., not including the effect of random peculiar velocities and redshift errors. The r_0 value (the correlation length of the projected 2pcf) reported in their Table 5 would suggest, instead, a higher bias ($\sim$5) when derived assuming that $w_{\rm p}(r_{\rm p})$ is modeled by a power law with index $\gamma = -2$ in the range $r_{\rm p} = 4$–$30\,h^{-1}$ Mpc.

At a slightly lower redshift, Francke et al. (2008) estimated the correlation function of a small sample of X-ray AGNs with $L_{\rm bol} \sim 10^{44.8}$ erg s^{-1}, in the Extended *Chandra* Deep Field South (ECDFS). Given the small number of sources, they only infer a minimum mass of halos hosting X-ray ECDFS AGNs of log $M_{\rm min} = 12.6^{+0.5}_{-0.8}\,h^{-1}\,M_{\odot}$ (based on Sheth et al. 2001 formalism). Our result is in agreement with this study at $z \sim 3$, but measured with higher accuracy.

Recently, Ikeda et al. (2015) investigated the clustering properties of low-luminosity quasars at $z \sim 4$ using the cross-correlation function of quasars and LBGs in the COSMOS field. They estimated the bias factor for a spectroscopic sample of 16 quasars and a total sample of 25 quasars including sources with photometric redshifts. They obtained a 86% upper limit for the bias of 5.63 and 10.50 for the total and spectroscopic sample, respectively.

5.3. Comparison to Theoretical Models

Figure 6 shows the predicted evolution of the AGN bias as a function of the bolometric luminosity, computed according to the framework of the growth and evolution of BHs presented in Shen (2009, see also Shankar et al. 2010) at $z = 3$ and 3.5 Their model assumes that quasar activity is triggered by major mergers of host halos (e.g., Kauffmann & Haehnelt 2000).

The major merger model is quite successful in predicting the bias of COSMOS AGNs at $z = 2.8$ as presented in Allevato et al. (2014), but underpredicts the bias re-estimated in the present work using the same AGN sample and $\pi_{\rm max} = 200\,h^{-1}$ Mpc. Given the large error bars, the model is in broad agreement with the bias of luminous quasars at similar redshifts as measured in Shen et al. (2009) and X-ray AGNs as estimated in Francke et al. (2008).

The prediction from the model slightly underpredicts our results for CCL AGNs at $z \sim 3.4$. We verified that the mismatch between merger models and our data does not change if a few parameters, such as the light-curve or the host halo mass distribution are changed in the major merger model. In fact, our result is still not well reproduced by the predictions from a modified Shen (2009) model in which the post-peak descending phase is cut out, with all other parameters held fixed. On the other hand, a model characterized by a steepening in the $L_{\rm peak}$–$M_{\rm h}$ relation mainly implying that preferentially

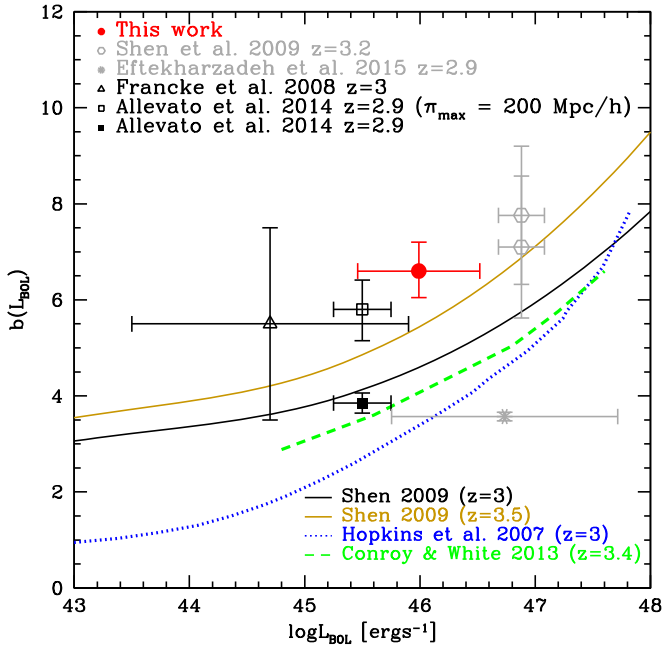

Figure 6. Predicted bias as a function of bolometric luminosity, computed according to Shen et al. (2009) at $z = 3$ (in black) and $z = 3.5$ (in gold), Hopkins et al. (2007a) at $z = 3$ (blue dotted line), and Conroy & White (2013) at $z = 3.4$ (green dashed line), compared to previously estimated bias factors for optically selected quasars at $z = 3.2$ (Shen et al. 2009, gray hexagon), X-ray selected AGNs at $z = 3$ (Francke et al. 2008, open triangle), *Chandra* and XMM-COSMOS AGNs at $z = 2.9$ as estimated in Allevato et al. (2014, filled black square) and as re-estimated in the present work (black empty square) and our results (red circle). The errors on the $L_{\rm bol}$ axis correspond to the dispersion of the bolometric luminosity distributions for the different subsets.

lower-luminosity quasars are now mapped to more massive, less numerous host DM halos, still underpredicts our results.

A similar mismatch has also been found for a sample of CCL AGNs at $z = 3$–6.5 in terms of observed number counts (Marchesi et al. 2016b). In fact, they verified that the reference model overproduces the observed number counts by a factor of 3 to 10, depending on the redshift.

We also compare the observations with the theoretical model presented in Hopkins et al. (2007a), which adopts the feedback-regulated quasar light-curve/lifetime models from Hopkins et al. (2006) derived from numerical simulations of galaxy mergers that incorporate BH growth. Even if we assume an evolution with redshift, this model underpredicts the bias factor of CCL AGNs.

A similar tension is also observed when comparing with the semi-empirical model presented in Conroy & White (2013). In the latter, the BH mass is linearly related to galaxy mass and connected to dark matter halos via empirically constrained relations. This model makes no assumption about what triggers the AGN activity and includes a scatter in the AGN luminosity–halo mass relation, contrary to Hopkins et al. (2007a) and Shen et al. (2009). Conroy & White (2013) show that this semi-empirical model naturally reproduces the clustering properties of quasars at $z < 3$, but shows some tension at higher redshift. They argue that this disagreement can be explained if AGNs have a duty cycle close to unity at $z > 3$, indicating that we approach the era of rapid BH growth in the early universe.

Recently, Gatti et al. (2016) used advanced semi analytic models (SAMs) of galaxy formation, coupled to halo occupation modeling, to investigate AGN triggering mechanisms such as galaxy interactions and disk instabilities. They compared the predictions with high redshift clustering measurements from Allevato et al. (2014), Shen et al. (2009), and Eftekharzadeh et al. (2015). Their SAMs underpredict the bias of luminous quasars shown in Shen et al. (2009). The mismatch is reduced when the models are compared to Eftekharzadeh et al. (2015). They pointed out that, irrespective of the exact implementations in their SAMs, at low-z moderate-luminosity AGNs ($L_{\rm bol} \sim 10^{44–46}$ erg s^{-1}) mainly inhabit halos with masses of $\sim 10^{12–13}\ M_\odot$ for both galaxy interaction and disk instabilities models (even if disk instabilities do not trigger the most luminous AGNs with $L_{\rm bol} \geqslant 10^{47}$ erg s^{-1}). At higher redshift ($z \sim 2.5$), structures with masses greater than $M_h > 10^{13}\ M_\odot$ become significantly rarer, relegating active galaxies to live mainly in less massive environments. Moreover, in all models, only galaxies with stellar masses above $10^{11}\ M_\odot$ would be able to host AGNs with luminosities of $L_{\rm bol} \sim 10^{46}$ erg s^{-1} and would be highly biased, such as COSMOS AGN at $z > 2$–3. This would imply that the characteristic $M_{\rm star}/M_{\rm h}$ ratio in AGN hosts should increase with lookback time, as expected from basic considerations on number densities evolution between the halo mass function and AGN luminosity function (e.g., Shankar et al. 2010).

6. CONCLUSIONS

We use the new CCL catalog to probe the projected and redshift-space 2pcf of X-ray selected AGNs for the first time at $2.9 \leqslant z \leqslant 5.5$, using the generalized clustering estimator based on phot-z Pdfs in addition to any available spec-z. We model the clustering signal with the two-halo model and we derive the bias factor and the typical mass of the hosting halos. Our key results are as follows.

(1) At $z \sim 3.4$, CCL AGNs have a bias of $b = 6.6^{+0.60}_{-0.55}$, which corresponds to a typical mass of the hosting halos of $\log M_{\rm h} = 12.83^{+0.12}_{-0.11}\ {\rm h}^{-1}\ M_\odot$. A similar bias is derived using the z-space 2pcf, modeled including the typical phot-z error $\sigma_z = 0.052$ of our sample. This confirms that the convergence of the projected 2pcf observed only at large scales ($\pi_{\rm max} \geqslant 200\ {\rm h}^{-1}$ Mpc) is due to large phot-z errors.

(2) A slightly larger bias $b = 7.5^{+1.6}_{-1.7}$ (but consistent within the error bars) is found using a sample of 107 CCL AGNs with known spec-z. The modeling of $\xi(s)$ suggests that this larger bias can be explained assuming that spec-zs are affected by errors of the order of $\sigma_z = 0.02$–0.025. This would explain the convergence of the projected 2pcf surprisingly observed only at $\pi_{\rm max} \geqslant 200\ {\rm h}^{-1}$ Mpc, even when phot-zs are not included in the analysis. However, given the low statistics smaller spec-z errors and then bias cannot be ruled-out.

(3) We estimate the bias factor for the sample of 346 XMM and *Chandra* AGNs used in Allevato et al. (2014) using $\pi_{\rm max} = 200\ {\rm h}^{-1}$ Mpc in estimating the projected 2pcf and then accounting for the large phot-z errors. In particular, we found $b = 5.8^{+0.61}_{-0.55}$, which is significantly larger than the AGN bias measured in Allevato et al. (2014) and corresponds to $\log M_{\rm h} = 12.92^{+0.13}_{-0.18}$ at $z = 2.8$.

(4) Our results suggest only a slight increase of the bias factor of COSMOS AGNs at $z \gtrsim 3$, with the typical hosting halo mass of moderate-luminosity AGNs almost constant with redshift and equal to $\log M_{\rm h} = 12.92^{+0.13}_{-0.18}$ at $z = 2.8$ and $\log M_{\rm h} = 12.83^{+0.12}_{-0.11}$ at $z \sim 3.4$, respectively.

(5) The observed redshift evolution of the bias of COSMOS AGNs implies that moderate-luminosity AGNs still inhabit group-sized halos, but are slightly less massive than observed in different independent studies using X-ray AGNs at $z \leqslant 2$.
(6) Theoretical models presented in Shen et al. (2009) and Hopkins et al. (2007a) that assume AGN activity mainly triggered by major mergers of host halos underpredicts our results at $z \sim 3.4$ for CCL AGNs with means of $L_{\rm bol} \sim 10^{46}\,{\rm erg\,s^{-1}}$. A similar tension is also observed when comparing to the semi-empirical models presented in Conroy & White (2013). In the latter model, this disagreement can be explained if AGNs have a duty cycle approaching unity at $z > 3$. On the other hand, following the SAMs presented in Gatti et al. (2016), in both galaxy interaction and disk instability models, only galaxies with stellar masses above $10^{11}\,M_{\odot}$ would be able to host AGNs with luminosities of $L_{\rm bol} \sim 10^{46}\,{\rm erg\,s^{-1}}$ and would be highly biased, such as COSMOS AGN at $z > 2$–3.

Only future facilities, like the X-ray Surveyor (Vikhlinin 2015) and Athena (PI K. P. Nandra), will be able to collect sizable samples (∼1000 s) of low-luminosity ($L_X < 10^{43}\,{\rm erg\,s^{-1}}$) AGNs at $z > 3$ (Civano 2015), allowing us to explore the clustering for significantly less luminous sources and to test AGN triggering scenarios at different AGN luminosities.

We thank the anonymous referee for helpful comments. We gratefully thank Federico Marulli for helpful discussions and input. We acknowledge the contributions of the entire COSMOS collaboration consisting of more than 100 scientists. More information on the COSMOS survey is available at http://cosmos.astro.caltech.edu/. V.A. and A.F. wish to acknowledge Finnish Academy award, decision 266918. This work was supported in part by NASA *Chandra* grant number GO3-14150C and also GO3-14150B (F.C., S.M., V.A., H.S.). R.G. acknowledges the receipt of NASA Grant NNX15AE61G. T.M. is supported by UNAM-DGAPA Grant PAPIIT IN104216 and CONACyT Grant Cientifica Basica 179662. K.S. gratefully acknowledges support from Swiss National Science Foundation Grant PP00P2_138979/1.

REFERENCES

Allevato, V., Finoguenov, A., Cappelluti, N., et al. 2011, ApJ, 736, 99
Allevato, V., Finoguenov, A., Civano, F., et al. 2014, ApJ, 796, 4
Bonoli, S., Marulli, F., Springel, V., et al. 2009, MNRAS, 396, 423
Bournaud, F., Dekel, A., Teyssier, R., et al. 2011, ApJ, 741, 33
Cappelluti, N., Brusa, M., Hasinger, G., et al. 2009, A&A, 497, 635
Cisternas, M., Jahnke, K., Inskip, K. J., et al. 2011, ApJ, 726, 57
Civano, F. 2015, in X-Ray Vision Workshop: Probing the universe in Depth and Detail with the X-Ray Surveyor (X-Ray Vision Workshop) (Washington, DC: National Museum of the American Indian), 22
Civano, F., Elvis, M., Brusa, M., et al. 2012, ApJS, 201, 30
Civano, F., Marchesi, S., Comastri, A., et al. 2016, ApJ, 819, 62
Coil, A. L., Georgakakis, A., Newman, J. A., et al. 2009, ApJ, 701, 1484
Conroy, C., & White, M. 2013, ApJ, 762, 70
Croom, Scott M., Boyle, B. J., Shanks, T., et al. 2005, MNRAS, 356, 415
Davis, M., & Peebles, P. J. E. 1983, ApJ, 267, 465
Dekel, A., Sari, R., & Ceverino, D. 2009, ApJ, 703, 785
Efstathiou, G., Bond, J. R., & White, S. D. M. 1992, MNRAS, 258, 1
Eftekharzadeh, S., Myers, A. D., White, M., et al. 2015, MNRAS, 453, 2779
Elvis, M., Civano, F., Vignani, C., et al. 2009, ApJS, 184, 158
Fanidakis, N., Georgakakis, A., Mountrichas, G., et al. 2013, MNRAS, 435, 679
Francke, H., Gawiser, E., Lira, P., et al. 2008, ApJ, 673, 13
Gatti, M., Shankar, F., Bouillot, V., et al. 2016, MNRAS, 456, 1073
Genzel, R., Burkert, A., Bouché, N., et al. 2008, ApJ, 697, 59
Georgakakis, A., Coil, A. L., Laird, E. S., et al. 2009, MNRAS, 397, 623
Georgakakis, A., Mountrichas, G., Salvato, M., et al. 2014, MNRAS, 443, 3327
Gilli, R., Daddi, E., Zamorani, G., et al. 2005, A&A, 430, 811
Gilli, R., Zamorani, G., Miyaji, T., et al. 2009, A&A, 494, 33
Hamana, T., Yoshida, N., & Suto, Y. ApJ, 568, 455
Hickox, R. C., Jones, C., & Forman, W. R. 2009, ApJ, 696, 891
Hickox, R. C., Myers, A. D., Brodwin, M., et al. 2011, ApJ, 731, 117
Hickox, R. C., Wardlow, J. L., Smail, I., et al. 2012, MNRAS, 421, 284
Hopkins, P. F., Hernquist, L., Cox, T. J., et al. 2006, ApJ, 163, 1
Hopkins, P. F., Hernquist, L., Cox, T. J., & Keres, D. 2008, ApJ, 175, 365
Hopkins, P. F., Lidz, A., Hernquist, L., et al. 2007a, ApJ, 662, 110
Hopkins, P. F., Richards, G. T., & Henquist, L. 2007b, ApJ, 654, 731
Ikeda, H., Nagao, T., Taniguchi, Y., et al. 2015, ApJ, 809, 138
Kaiser, N. 1987, MNRAS, 227, 1
Kauffmann, G., & Haehnelt, M. 2000, MNRAS, 311, 576
Kocevski, D. D., Faber, S. M., Mozena, M., et al. 2012, ApJ, 744, 148
Kormendy, J., & Bender, R. 2011, Natur, 469, 377
Kormendy, J., & Richstone, D. 1995, ARA&A, 33, 581K
Koutoulidis, L., Plionis, M., Georgantopoulos, I., & Fanidakis, N. 2013, MNRAS, 428, 1382
Krumpe, M., Miyaji, T., & Coil, A. L. 2010, ApJ, 713, 558
Landy, S. D., & Szalay, A. S. 1993, ApJ, 412, 64
Li, C., Kauffmann, G., Wang, L., et al. 2006, MNRAS, 373, 457
Lilly, S. J., Le Févre, O., Renzini, A., et al. 2007, ApJS, 172, 70
Marchesi, S., Civano, F., Elvis, M., et al. 2016a, ApJ, 817, 34
Marchesi, S., Lanzuisi, G., Civano, F., et al. 2016b, ApJ, in press, arXiv:160805149M
Marconi, A., Risaliti, G., Gilli, R., et al. 2004, MNRAS, 351, 169
Menci, N., Cavaliere, A., Fontana, A., et al. 2003, ApJ, 587, 63
Menci, N., Fiore, F., Perola, G. C., & Cavaliere, A. 2004, ApJ, 606, 58
Mendez, A. J., Coil, A. L., Aird, J., et al. 2016, ApJ, 821, 55
Miyaji, T., Zamorani, G., Cappelluti, N., et al. 2007, ApJS, 172, 396
Mountrichas, G., & Georgakakis, A. 2012, MNRAS, 420, 514
Mountrichas, G., Georgakakis, A., Finoguenov, A., et al. 2013, MNRAS, 430, 661
Mullaney, J. R., Pannella, M., Daddi, E., et al. 2012, MNRAS, 419, 95
Myers, A. D., White, M., & Nicholas M, B. 2009, MNRAS, 399, 2279
Neistein, E., & Netzer, H. 2014, MNRAS, 437, 3373
Peacock, J. A., Cole, S., Norberg, P., et al. 2001, Natur, 410, 169
Peebles, P. J. E. 1980, The Large Scale Structure of the universe (Princeton, NJ: Princeton Univ. Press)
Porciani, C., & Norberg, P. 2006, MNRAS, 371, 1824
Rosario, D. J., Mozena, M., Wuyts, S., et al. 2013, ApJ, 763, 59
Ross, N. P., Shen, Y., Strauss, M. A., et al. 2009, ApJ, 697, 1634
Salvato, M., Ilbert, O., Hasinger, G., et al. 2011, ApJ, 742, 61
Scannapieco, E., & Oh, S. P. 2004, ApJ, 608, 62
Schawinski, K., Simmons, B. D., Urry, C. M., Treister, E., & Glikman, E. 2012, MNRAS, 425, 61
Schawinski, K., Treister, E., Urry, C. M., et al. 2011, ApJ, 727, 31
Scoville, N., Abraham, R. G., Aussel, H., et al. 2007, ApJS, 172, 38
Sereno, M., Veropalumbo, A., Marulli, F., et al. 2015, MNRAS, 449, 4147
Shankar, F. 2010, IAUS, 267, 248
Shankar, F., Weinberg, D. H., & Shen, Y. 2010, MNRAS, 406, 1949
Shanks, T., Croom, S. M., Fine, S., Ross, N. P., & Sawangwit, U. 2011, MNRAS, 416, 650
Shen, Y. 2009, ApJ, 704, 89
Shen, Y., Strauss, M. A., Ross, N. P., et al. 2009, ApJ, 697, 1656
Shen, Y., Strauss, M. A., Oguri, M., et al. 2007, AJ, 133, 2222
Sheth, R. K., Mo, H. J., & Tormen, G. 2001, MNRAS, 323, 1
Starikova, S., Cool, R., Eisenstein, D., et al. 2011, ApJ, 741, 15
Tinker, J. L., Robertson, B. E., Kravtsov, A. V., et al. 2010, ApJ, 724, 878
Treister, E., Schawinski, K., Urry, C. M., & Simmons, B. D. 2012, ApJ, 758, 39
Trump, J. R., Impey, C. D., Elvis, M., et al. 2009, ApJS, 696, 1195
Trump, J. R., Impey, C. D., McCarthy, P. J., et al. 2007, ApJS, 172, 383
van den Bosch, F. C. 2002, MNRAS, 331, 98
Vikhlinin, A. 2015, in X-Ray Vision Workshop: Probing the universe in Depth and Detail with the X-Ray Surveyor (X-Ray Vision Workshop) (Washington, DC: National Museum of the American Indian), 24
Villforth, C., Hamann, F., Rosario, D. J., et al. 2014, MNRAS, 439, 3342
Volonteri, M., Haardt, F., & Madau, P. 2003, ApJ, 582, 559
Zehavi, I., Eisenstein, D. J., Nichol, R. C., et al. 2005, ApJ, 621, 22